Functional Biomaterials Surfaces

JOURNAL OF
biomaterials
applications

Journal of Biomaterials Applications
2018, Vol. 33(5) 725–740


Article reuse guidelines:
sagepub.com/journals-permissions
DOI: 10.1177/0885328218809911
journals.sagepub.com/home/jba
SAGE

Improved corrosion resistance of commercially pure magnesium after its modification by plasma electrolytic oxidation with organic additives

Monica Echeverry-Rendon[1,2,3], Valentina Duque[2], David Quintero[2], Sara M Robledo[3], Martin C Harmsen[1] and Felix Echeverria[2]

Abstract

The optimal mechanical properties render magnesium widely used in industrial and biomedical applications. However, magnesium is highly reactive and unstable in aqueous solutions, which can be modulated to increase stability of reactive metals that include the use of alloys or by altering the surface with coatings. Plasma electrolytic oxidation is an efficient and tuneable method to apply a surface coating. By varying the plasma electrolytic oxidation parameters voltage, current density, time and (additives in the) electrolytic solution, the morphology, composition and surface energy of surface coatings are set. In the present study, we evaluated the influence on surface coatings of two solute additives, i.e. hexamethylenetetramine and mannitol, to base solutes silicate and potassium hydroxide. Results from in vitro studies in NaCl demonstrated an improvement in the corrosion resistance. In addition, coatings were obtained by a two-step anodization procedure, firstly anodizing in an electrolyte solution containing sodium fluoride and secondly in an electrolyte solution with hexamethylenetetramine and mannitol, respectively. Results showed that the first layer acts as a protective layer which improves the corrosion resistance in comparison with the samples with a single anodizing step. In conclusion, these coatings are promising candidates to be used in biomedical applications in particular because the components are non-toxic for the body and the rate of degradation of the surface coating is lower than that of pure magnesium.

Keywords

Magnesium, plasma electrolytic oxidation, hexamethylenetetramine, mannitol, corrosion resistance

Introduction

Magnesium (Mg) is a lightweight material with a favorable ductility and easy processability. These characteristics render Mg widely used in aerospace and automotive industries, in the manufacture of electronic devices and also in the biomedical field. However, its high chemical reactivity is a major obstacle to use this material as it is easily corroded. For instance, in biomedical applications, the biocompatibility of a metallic Mg-based implant is compromised by the accumulation of hydrogen gas and rapid changes in pH in the environment during its degradation. The use of Mg alloys or of surface coatings decrease the degradation rate and thus alleviate reactivity-related problems. Spontaneous oxidation of Mg in ambient air produces a protective (oxide) surface layer on Mg as well as other metals, such as Ti and Al. However, this oxide layer is too thin to provide long-term protection to the metal against accelerated degradation. Therefore, various techniques such as plasma electrolytic oxidation

[1]University of Groningen, University Medical Center Groningen, Department of Pathology and Medical Biology, Hanzeplein, Groningen, the Netherlands
[2]Centro de Investigación, Innovación y Desarrollo de Materiales CIDEMAT, Facultad de Ingeniería, Universidad de Antioquia UdeA, Calle 70 No. 52-21, Medellín, Colombia
[3]Programa de Estudio y Control de Enfermedades Tropicales PECET, Instituto de Investigaciones Médicas, Facultad de Medicina, Universidad de Antioquia UdeA, Calle 70 No. 52-21, Medellín, Colombia

Corresponding author:
Monica Echeverry-Rendon, University of Groningen, University Medical Center Groningen, Department of Pathology and Medical Biology, Hanzeplein 1, EA11, NL-9713 GZ Groningen, the Netherlands.
Email: monicaecheverryr@gmail.com

(PEO) also known as micro-arc oxidation (MAO) are used to add a protective oxide layer, i.e. surface coating, in a controlled way.[1–3] PEO comprise a modified conventional anodization in which punctual micro-discharges occur on the Mg surface, accompanied with gas evolution, forming a surface film. Subsequently, the high voltage causes a dielectric breakdown and stable thick surface coating. Modification of parameters such as voltage, current density, electrolyte solution composition and discharge time determine the morphology, thickness, composition and physiochemical properties of the surface coating. Together, these characteristics directly impact the overall corrosion resistance of the material. The influence of varying morphology and microstructure of the coatings depends on the additives that alter the conductivity of the solutes. This affects the formation of the anodic surface layer.[4] In general, anodization by PEO requires a base electrolytic solution that contains silicates,[5–7] phosphates[2,8,9] or aluminates.[2] Frequently used are base solutions of sodium metasilicate or potassium hydroxide.[10] The improvement of the corrosion resistance can be achieved via other additives such as borates, sulfate, glycerol, sodium citrate, ammonium, phosphate, ethylene glycol, among others[8,11–14] to the solute help to generate new phases in the surface coating.[15] PEO is a simple, low-cost, reproducible and reliable technique to modify surfaces of metals like titanium, aluminum, Mg.[16–19]

It is clear that further improvement of surfaces of chemically pure (c.p) Mg by PEO is warranted. In the present study we investigated three additives, one inorganic i.e. sodium fluoride (NAF)[15] and two novel organic additives i.e. hexamethylenetetramine (HMT) and mannitol (MAN). These compounds are expected to influence the electrical conductivity of the solution without altering the basic $MgO/Mg(OH)_2$ composition of the final surface coating. The non-toxic nature of organic compounds HMT and MAN render these suitable for biomedical implant modification. The aim of this study was to evaluate the corrosion resistance of Mg surface coatings obtained by PEO in presence of the additives HMT and MAN in the electrolyte solution and compare them with NAF. In addition, we hypothesize that building up a surface coating in two consecutive PEO steps with different solute and additives formulations will provide an additional opportunity to fine-tune the composition and physicochemical properties surface coatings of c.p Mg. This approach was derived from the hypothesis that the first relatively thin layer made in an NAF additive could offer corrosion protection, because it passivates Mg surfaces. This NAD-derived layer could facilitate the formation of a thicker layer driven by additives HMT or MSN and provide a better corrosion protection.

Materials and methods

Sample processing

Commercially pure Mg (99.9%) samples with dimensions of 1 cm × 1 cm and 1 mm thickness were polished with increasing size (up to 1000 grade) silicon carbide paper. Next, samples were sonicated in acetone for 30 min in an ultrasonic bath.

Anodization of the samples

The anodization setup consisted of an electrolytic cell in which a stainless-steel beaker with the electrolytic solution was used as cathode and the immersed Mg sample was used as anode and connected to a direct current power supply (Kepco BHK 500–0.4 MG). The base electrolytic solution consisted of sodium metasilicate (0.1 M $Na_2SiO_3.9H_2O$) and potassium hydroxide (0.07 M KOH). Three different additives were evaluated; one commonly used i.e. 0.2 M sodium fluoride (0.2 M, NAF) and hexamethylenetetramine (0.07 M $C_6H_{12}N_4$, HMT) and mannitol (0.05 M $C_6H_{14}O_6$, MAN). NAF samples were anodized at galvanostatic mode and for HMT and MAN potentiostatic mode was used. In Table 1, the operational parameters are summarized.

In addition, samples were processed using a two-step anodizing process as shown in Table 2. First, samples were anodized following the protocol used for NAF and posteriorly samples were anodized for a second time with HMT or MAN at potentiostatic mode.

Table 1. PEO conditions tested for anodization of c.p Mg surfaces in various electrolytes and additives. In all cases anodization was carried out for 600 s.

Abbreviation	Solution Composition	Current density	Voltage
NAF	0.07 M KOH + 0.1 M $Na_2SiO_3.9H_2O$ + 0.2 M NaF	104.16 $mA.cm^{-2}$	–
HMT	0.07 M KOH+ 0.1 M $Na_2SiO_3.9H_2O$+ 0.07 M $C_6H_{12}N_4$	–	320 V
MAN	0.07 KOH + 0.1 M $Na_2SiO_3.9H_2O$ + 0.05 M $C_6H_{14}O_6$	–	350 V

PEO: plasma electrolytic oxidation; NAF: sodium fluoride; HMT: hexamethylenetetramine; MAN: mannitol.

Table 2. Parameters employed to form the two-step anodic coatings. Both anodization steps were carried out for 600 s.

	Anodization 1	Anodization 2
Electrolytes	Current Density ($mA.cm^{-2}$)	Voltage (V)
NAF-HMT	104.16	320
NAF-MAN	104.16	350

NAF: sodium fluoride; HMT: hexamethylenetetramine; MAN: mannitol.

Surface characterization

The surface of the obtained coatings and its respective cross sections were observed by scanning electron microscopy (SEM) (JEOL JSM 6940LV). The chemical composition of the coatings was analyzed by energy dispersive spectroscopy (EDS) and by X-ray diffraction (XRD) by using an X-Pert Philips PW 3040/60 instrument with Cu Kα radiation with a scan range in 2θ from 20° to 90°. Grazing incidence X-ray diffraction (GIXD) patterns were taken with a 0.05° step at an incident angle α of 2°. The phases present in the coatings were identified in the HighScore Plus software by comparison with data in the ICSD database. Topography and surface morphology were assessed by using atomic force microscopy (AFM) (MFP-3D Infinity, Asylum Research). Areas of $50\,\mu m \times 50\,\mu m$ were scanned in contact mode at a rate of 0.3 Hz, using a TR400PB tip (tip radius 42 nm, spring constant of 0.1). To quantify surface roughness, average amplitude in the height direction were measured at different points with respect of the central line. Some of the most commonly reported parameters for roughness are R_a and R_q, R_a (arithmetic mean roughness) is the average of the heights calculated on the entire measurement of the length or area. R_a is frequently used to describe the roughness of machined surfaces. This is useful to detect general variations in the characteristic heights of the profile and to monitor and establish manufacturing processes. On the other hand, R_q or mean root mean square (RMS) is the quadratic mean of the deviations of the roughness profile from the midline along the evaluation length, this parameter is more sensitive than R_a due to the large deviations from the mean. AFM image analysis was carried out with Asylum Research Software to obtain R_a and R_q values. Additionally, the percentage of porosity of each sample was calculated by using ImageJ 1.48v (Wayne Rasband National Institutes of Health, USA) and reported as % area.

Surface energy

Wettability of samples was measured by using a Goniometer/Tensiometer Ramé-hart Model 250 Standard. For this, a droplet of deionized water was deposited on each surface ($n = 5$). This process was performed in three independently anodized samples. For the surface energy calculations, the average of the measurements of contact angle for water were used. Surface energy (γ_S) was calculated based on the Neuman method (equation 1)[20–23]

$$\cos\theta = 2\left(\frac{\gamma_S}{\gamma_L}\right)^{0.5}\exp\left[-\beta(\gamma_L - \gamma_S)^2\right] - 1 \qquad (1)$$

where $\beta = 0.0001247\ (m^2/mJ)^2$, $\gamma_L = 72.8\ mJ/m^2$ [24–26] and θ (contact angle) was as measured previously and with the respective numerical iterations required.

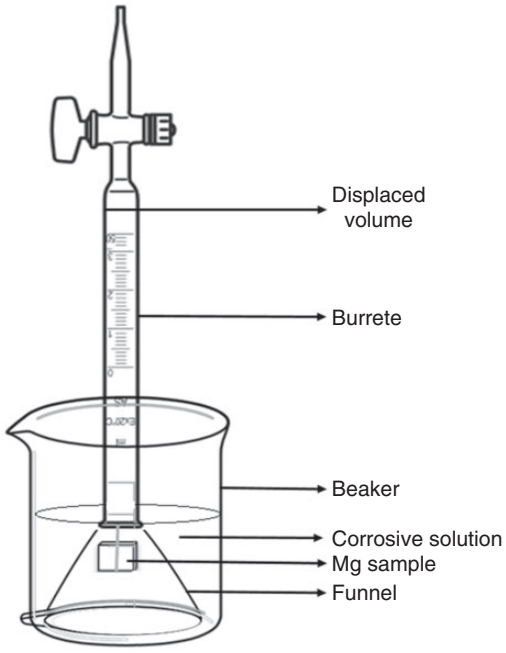

Figure 1. Schematic of the setup used for the hydrogen evolution measurement.

Evaluation of corrosion resistance

Hydrogen evolution was used to measure the corrosion resistance of the different specimens. For this purpose, a sample was placed in an inverted burette filled with 0.1 M NaCl[27,28] as is shown in Figure 1. The displacement of the liquid by production of hydrogen gas was read daily for one month. Hydrogen evolution rate V_H ($mL[cm^{-2}.day^{-1}]$) was converted into the degradation rate $P_H(mm.year^{-1})$ using the equation $P_H = 2.279\,V_H$.[27,29–31] Finally, the samples were analyzed in both top and cross-section views by SEM at the end of the hydrogen evolution test.

Biological assays

Cytotoxicity test. Dermal fibroblasts (PK48) were seeded at a concentration of 5000 cells/cm^2 in 24-well plates in

DMEM (Lonza) supplemented with 10% SBF (Lonza), 1% penicillin/streptomycin (Gibco) and 2 mM l-glutamine (Lonza) until confluency. Next, samples were added to each well and incubated at 37°C, 5% CO_2 and 98% humidity. Cell proliferation was measured at 24 h and 72 h with the Alamar Blue assay. For this, Alamar Blue (Invitrogen) solution was added to each well at a 1:10 ratio with respect to the volume of the medium and incubated at 37°C for 90 min. Then the supernatant was transferred to another plate and fluorescence was read in a fluorometer (Varioskan, Thermo scientific) at an excitation wavelength of 530 nm and an emission of 590 nm. Fresh medium was added to the cells. Each experiment was performed in triplicate and the values were normalized according to the measurement obtained at 24 h to calculate the percentage of increasing/decreasing population after 72 h.

Cell-material interaction. Human osteoblastic cell line Saos-2 (HTB-85, ATTC, USA) growing in McCoy medium (Sigma-Aldrich, Missouri, USA), supplemented with 10% FBS (Lonza, NJ, USA), 1% penicillin/streptomycin (Gibco, Massachusetts, USA) and 2 mM l-glutamine (Lonza, NJ, USA) was maintained under culture until confluency. Next, cells were detached using trypsin at 37°C for 5 min. About 50,000 cells were concentrated in 100 µL of medium and this volume was loaded onto each sample and incubated for 30 min to allow cells to attach. After that, 1 mL of fresh medium was gently added and cells were incubated at 37°C, 5% CO_2 for 48 h. Then, samples were rinsed twice with PBS and fixed in 4% paraformaldehyde in PBS at room temperature for 30 min. Next, cells were permeabilized with 0.5% triton X-100 for 15 min and blocked with 5% BSA-PBS overnight. Finally, staining for actin was carried out with 5 µg/mL Phalloidin-TRITC (P1951, Sigma, Missouri, USA) while nuclei were stained with DAPI (D9542, Sigma, Missouri, USA). Cells were assessed using a fluorescence microscope (Nikon LABOPHOT-2) at a ×10 objective magnification.

Hemolysis test. Citrated human blood was drawn and used for the hemolysis test. For this the citrated blood was diluted with saline solution in a ratio of 4:5. After that, material samples with and without coating were dipped in tubes containing 10 mL of saline solution and incubated at 37°C for 30 min. Next, 0.2 mL of diluted blood was added to each tube, mixed carefully and incubated at 37°C for 60 min. Then, tubes were centrifuged at $700 \times g$ for 5 min. Supernatants were transferred to a plate and absorbance was read at 545 nm. Deionized water and saline solution were used as positive and negative controls, respectively. Hemolysis was calculated based on the equation (2)

$$Hemolysis = \frac{OD(test) - OD(negative\ control)}{OD(positive\ control) - OD(negative\ control)} \times 100 \quad (2)$$

Thrombin generation assay. Anodized and untreated Mg samples with dimensions of 0.1×0.5 cm $\times$ 0.5 cm were used for the thrombin generation assay (TGA). Low-density polyethylene (LDPE), polydimethylsiloxane (PDMS) and medical steel (MS) were used as reference materials. Reactions without material were used as negative control. Thrombin generation was determined with (Haemoscan, Groningen, The Netherlands) according to the manufacturer's protocol. Briefly, samples were incubated in modified plasma in triplicate. Then, TGA reagent was added to initiate thrombin generation. After that, samples were collected every 2 min for 21 min. Then concentration of thrombin was measured by a colorimetric technique produced by an enzymatic reaction by using a thrombin-specific chromogenic substrate. Samples were read at an optical density of 405 nm with 540 nm as reference wavelength. After obtaining the data, thrombin concentration and rate of thrombin generation were calculated for each sample based on a calibration curve and compared with the reference materials and negative control.

Results

Characterization of the coatings

The change of resp. voltage–time or current density–time of the anodizing process of c.p Mg using different electrolyte solutions is shown in Figure 2. The NAF samples were operated under galvanostatic mode. The curve shows that the breakdown voltage was around 90 V which was reached in 2 s, this step is directly related to the onset of the generation of the oxide surface coating production of the barrier layer. Once this value was reached, the voltage oscillated around 150 V for the remainder of the experiment, while the thickness of the coating steadily increased. In contrast, HMT and MAN anodizations were operated at potentiostatic mode. Once the process started, current density increased until it reached 170 mA.cm^{-2}. Samples remained at this value for 35 s for the HMT and 40 s for MAN. Then the current decreased to 3 mA.cm^{-2} in 35 s for HMT and in 80 s for MAN. For the two-step anodization, NAF-HMT and NAF-MAN responded similarly: a maximum current of 170 mA·cm^{-2} was

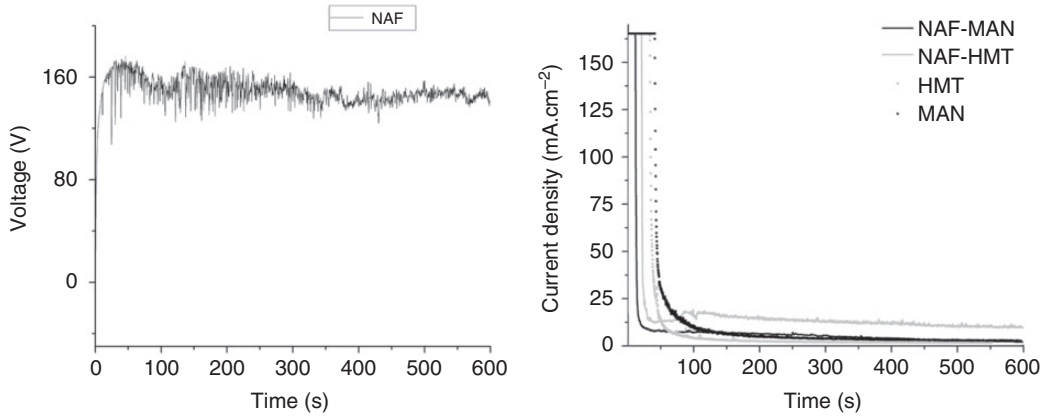

Figure 2. Current density–time and voltage–time responses during PEO of c.p Mg with different electrolyte additives in galvanostatic (NAF) or potentiostatic (HMT, NAF-HMT, MAN and NAF-MAN) mode.
PEO: plasma electrolytic oxidation; NAF: sodium fluoride; HMT: hexamethylenetetramine; MAN: mannitol.

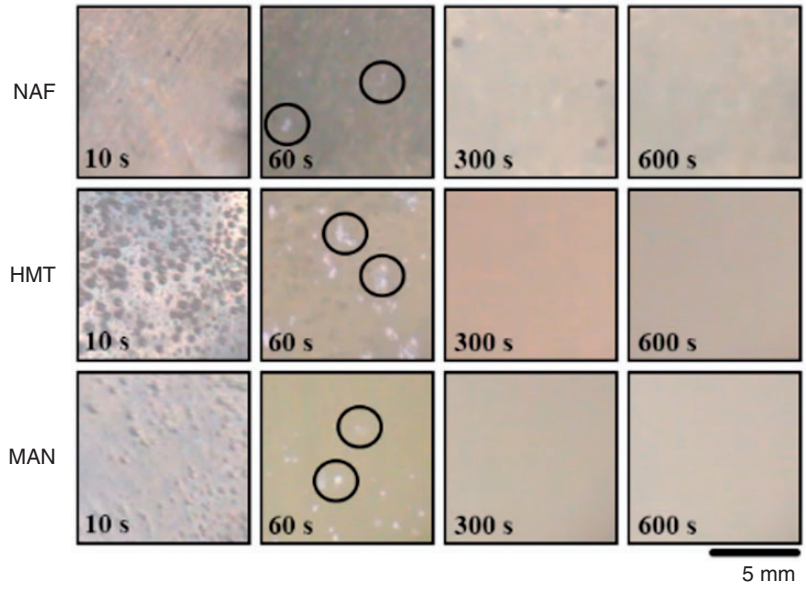

Figure 3. Micro-discharge appearance during different stages of PEO.
PEO: plasma electrolytic oxidation.

reached that was maintained for 22s for NAF-HMT and for 12 s for NAF-MAN. Next, in NAF-HMT the current decreased to 30 mA·cm^{-2} after 8 s and reached a steady-state level of 13 mA·cm^{-2}. For NAF MAN the current decreased to 60 mA·cm^{-2} after 14 s and reached a steady-state level of 5 mA·cm^{-2}.

Occurrence of sparks (micro discharges) at different stages of the process is shown in Figure 3. During the first 10 s of the PEO process, gas was formed on the surface, followed by micro-discharges in all conditions albeit these were challenging to visualize. In contrast to all other conditions, NAF additive produced the smallest and weakest micro-discharges which suggest that a compact coating was forming. In the potentiostatic PEO process, the micro-discharges density decreased due to the sharp incline of the current density when the potential reached a steady-state level.

Scanning electron micrographs of surfaces and cross sections are shown in Figure 4. The NAF-based surfaces consisted of non-uniform small pores approximately 0.4 μm in diameter and a circumference of approximately 1.2 μm. In cross section, the coating showed a low surface porosity comprising interconnected pores. The thickness of the layer was 3.2 $\pm$ 0.4 μm with a barrier layer of about 0.3 μm. In this sample, the polishing lines of the base material were also visible. The surface morphology of the

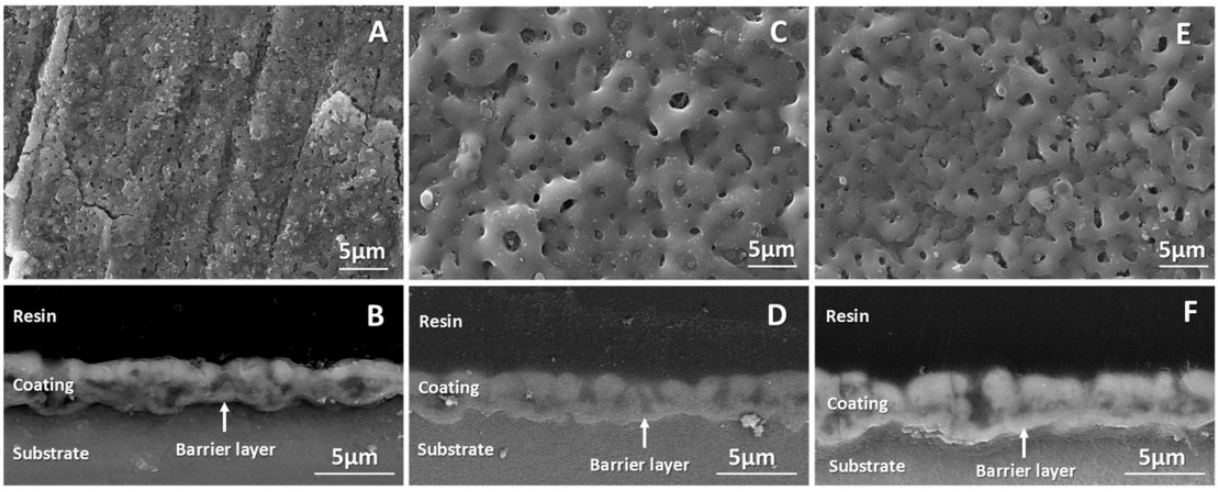

Figure 4. Surfaces and cross-section views of PEO-modified c.p Mg. NAF (a, b) coating shows a compact appearance, while HMT (c, d) and MAN (e, f) appeared to form porous coatings.
PEO: plasma electrolytic oxidation; NAF: sodium fluoride; HMT: hexamethylenetetramine; MAN: mannitol.

HMT-based coating consisted of uniformly distributed well-defined pores with a diameter of 1.3 ± 0.4 μm. The thickness of the coating was 2.9 ± 0.5 μm with a compact barrier layer of 0.7 ± 0.1 μm. Similarly, MAN-based coatings also showed a uniform distribution of pores, with a diameter of 1.3 ± 0.7 μm. The density of the pores on MAN-based surfaces was higher than on HMT-based surfaces. The cross section of the MAN showed a thin compact inner layer of 0.7 ± 0.1 μm superimposed by the porous layer reaching a combined thickness of 4.0 ± 0.5 μm.

Surfaces that were generated by a two-step anodization had a higher porosity than single anodized surfaces (Figure 5). NAF-HMT-based surfaces had multiple discontinuities that appeared to be formed by coalescing of pores. The average pore size was 1.4 ± 0.9 μm. The thickness of the surface coating was 3.2 ± 0.4 μm. For NAF-MAN the structure was more uniform and similar to the surface topographies obtained with single-step PEO with MAN. Although, the two-step PEO produced slightly larger pores, the average pore size was 1.3 ± 0.6 μm while the thickness of this coating was 4.0 ± 0.4 μm. The average thickness NAF-HMT-based and NAF-MAN-based two-step surfaces was, respectively, 0.6 ± 0.1 μm and 0.5 ± 0.1 μm. In these latter surfaces, the internal porosity was similar, while interconnected pores were located mostly directly above the barrier layer.

The chemical composition of the coatings was determined by XRD (Figure 6) and EDS; the XRD analyses were hampered by high intensity of the substrate-based peaks that hid surface coating-based peaks. A grazing angle of 2° allowed to characterize the crystalline composition of the anodic film. All the samples showed Mg oxide as the main crystalline phase. NAF-based surfaces showed two peaks corresponding to the presence of MgF_2 approximately 40 and 53° (Figure 6(a)). This was corroborated by EDS analyses which showed the presence of F and NAF-based surfaces (Table 3). In HMT-based surfaces, the XRD signal at 23° suggests the presence Mg_2SiO_4 (Figure 6(b)). Additional anticipated surface coating-based XRD signals were likely obscured by the strong signals from the Mg substrate. The EDS analysis also included signals from the substrate material, as observed by the high amounts of Mg detected. However, these values are useful to analyze the effect of the additives. This analysis evidenced a similar incorporation of silicon from the base anodizing solution for all samples, except for NAF-based surface coatings in which the signal or presence of Si was much lower and only allowed detection of fluoride.

The mean roughness (R_a) of the coatings with different anodic coatings ranged from 160 to 198 nm (Table 4). This was similar to untreated c.p Mg which had an R_a of 172 nm (Figure 7). Additionally, R_q values were similar for all the treatments and ranged from 205 nm to 256 nm (Table 4). Part of the observed surface topographies were remaining 'polishing' lines. These polishing artifacts were less evident for the thicker coatings generated with MAN and NAF-MAN as additive. However, both SEM and AFM show that surface morphology varied with anodization, these features will probably affect more other characteristics of the surface, such as wettability and cell-material interactions. The percentage of porosity (% area) for the samples were 72.97% for NAF, 39.36% for HMT, 31.39% for MAN, 31.09% for NAF-HMT and 44.75% for NAF-MAN.

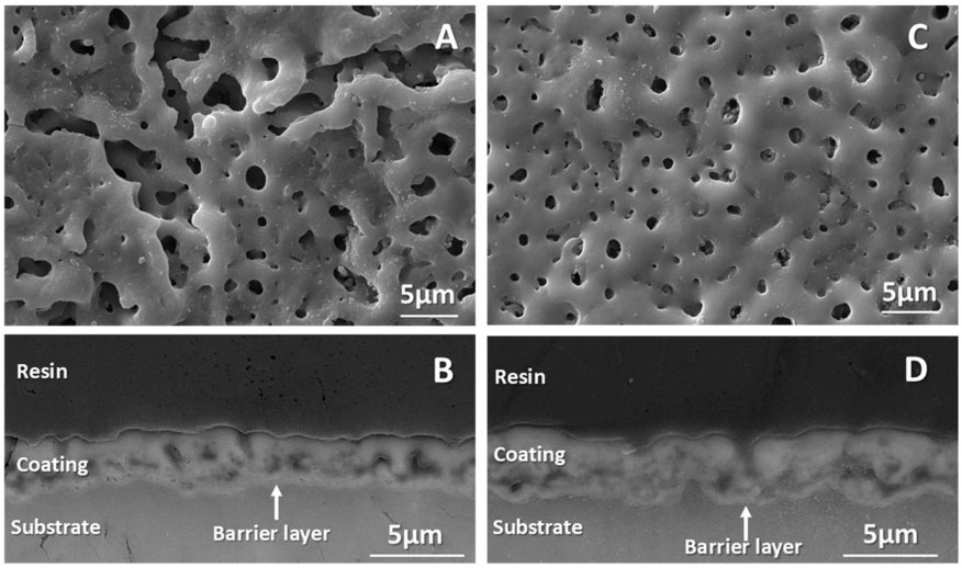

Figure 5. Morphology and cross section of two-step coatings. Interconnected pores are present on the surfaces of NAF-HMT (a and b) and NAF-MAN (c and d) samples.
PEO: plasma electrolytic oxidation; NAF: sodium fluoride; HMT: hexamethylenetetramine; MAN: mannitol.

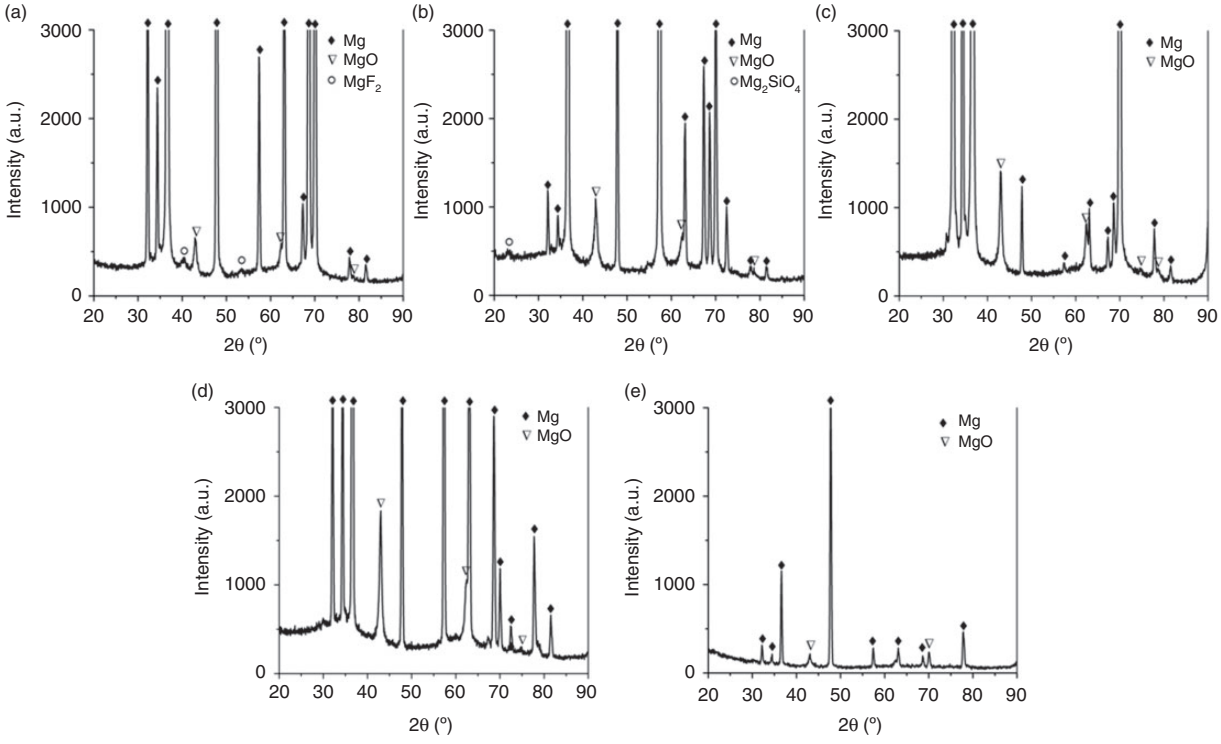

Figure 6. XRD patterns of samples of PEO-modified Mg samples. The main component of the all anodic films was Magnesium oxide (inverted triangles). NAF (a), HMT (b), MAN (c), NAF-HMT (d) and NAF-MAN (e).
XRD: X-ray diffraction; PEO: plasma electrolytic oxidation; NAF: sodium fluoride; HMT: hexamethylenetetramine; MAN: mannitol.

Wettability and surface energy

Wettability or contact angle is a feature of surfaces that is important for use in biomedical applications that require adherence of cells. Hydrophilic surface support deposition and adhesion of proteins, which promotes cell adhesion. The contact angle of c.p Mg was 81°, which means it had a hydrophobic surface.

The generation of surface coatings reduced the contact angle. The reduction was approximately 50% (range 30° to 54°) for coatings after single anodizing with additives NAF, HMT and MAN and for two-step coatings with NAF-HMT and NAF-MAN. These two-step generated surfaces had the lowest contact angles (approx. 3°) and were highly hydrophilic. It appeared that PEO by anodization caused lower contact angles than cationic PEO. According to these data, at lower contact angles, a higher surface energy and more affinity with interaction with liquids was facilitated (Table 4). It should be noted that, unexpectedly, surface roughness did not correlate with contact angle. In addition, two-step anodization with additives HMT and MAN virtually abolished the differences in contact angle observed after a single anodization.

Corrosion resistance

The corrosion resistance of the surface coatings was assessed by hydrogen evolution in NaCl for 1 month (Figure 8). All samples with surface modification had a lower corrosion rate in comparison to control c.p Mg. The degradation of c.p Mg showed a typical behavior with an initial fast degradation of maximally 0.10 mm. $year^{-1}$, with a slope of 0.02 mm.$year^{-1}$. After six days, the degradation gradually decreased due to the passivation, i.e. formation of a corrosion-resistant, protective, layer (Figure 8). Coated samples also corroded faster during the first hours of immersion with maximum values of around 0.09 mm·$year^{-1}$, 0.08 mm·$year^{-1}$ and 0.03 mm·$year^{-1}$ for NAF, HMT and MAN, respectively. Similar to c.p Mg, the NAF- and HMT-based surface-coated samples then slowed the degradation rate until reaching a steady state level of 0.032 mm·$year^{-1}$ and 0.016 mm·$year^{-1}$, respectively. In the case of MAN, after an initial increase, it maintained a similar corrosion rate of around 0.028 mm·$year^{-1}$ during all the test. Degradation profiles of two-step coatings were similar to single anodized coatings with a maximum corrosion rate of 0.09 mm·$year^{-1}$ for NAF-HMT and 0.03 mm·$year^{-1}$ for NAF-MAN. These samples reached the steady state degradation levels at about 0.006 mm·$year^{-1}$ for NAF-HMT and 0.003 mm $year^{-1}$ for NAF-MAN, which was approximately ten-fold lower than single anodized coatings. Of note, the degradation dynamics between e.g. single NAF anodized samples and two-step anodized samples differed, which allows to select for an initially faster corroding coating versus a lower but constantly degrading coating. The average corrosion rates for bare c.p Mg, NAF, HMT, MAN, NAF-HMT and NAF-MAN were 0.067 mm·$year^{-1}$, 0.033 mm·$year^{-1}$, 0.018 mm·$year^{-1}$, 0.025 mm·$year^{-1}$, 0.018 mm·$year^{-1}$ and 0.008 mm·$year^{-1}$, respectively.

Table 3. Composition of the coatings by EDS (% weight-mapping).

Sample	O	Mg	Si	F
NAF	8.1	89.0	1.5	1.4
HMT	12.1	82.2	5.7	–
MAN	18.8	76.1	5.1	–
NAF-HMT	7.8	87.4	4.8	–
NAF-MAN	7.8	86.8	5.4	–

EDS: energy dispersive spectroscopy; plasma electrolytic oxidation; NAF: sodium fluoride; HMT: hexamethylenetetramine; MAN: mannitol.

Finally, surfaces and cross sections of the samples were analyzed by SEM after one month of immersion (Figure 9). In samples anodized with NAF, HMT, MAN and NAF-MAN the structure and morphology of the coatings were conserved whereas samples anodized with NAF-HMT showed loss of the porous structure. The cracks observed in the surfaces are an artifact that is caused by the vacuum that is required to operate an SEM because these were not observed if surfaces were analyzed with AFM.

In order to quantify the magnitude of the corrosion, the area of the corrosion products layer (Figure 9) was calculated as an indicative parameter. The corrosion area was 73 μm^2 for NAF, 65 μm^2 for HMT and 40 μm^2 for MAN. For samples with two-step anodization, the corrosion area was 35 μm^2 for NAF-HMT and 22 μm^2 for NAF-MAN. The fastest degrading material i.e. bare c.p Mg had the highest corrosion

Table 4. Surface characteristics of the coatings of Mg obtained by PEO.

Sample	Ra (nm)	Rq (nm)	Thickness (μm)	Contact angle (°)	Surface energy (mJ·m^{-2})
NAF	167.1	214.6	3.2 ± 0.4	53.5 ± 3.9	51.7
HMT	187.9	232.9	4.2 ± 0.5	29.8 ± 1.6	64.5
MAN	160.6	205.0	5.1 ± 1.1	37.9 ± 0.1	60.5
NAFHMT	198.2	255.7	3.2 ± 0.4	8.7 ± 0.3	71.9
NAFMAN	167.5	209.6	4.0 ± 0.4	9.4 ± 0.4	71.8
Untreated c.p Mg	172.6	220.1	-	80.9 ± 6.5	34.9

PEO: plasma electrolytic oxidation; NAF: sodium fluoride; HMT: hexamethylenetetramine; MAN: mannitol.

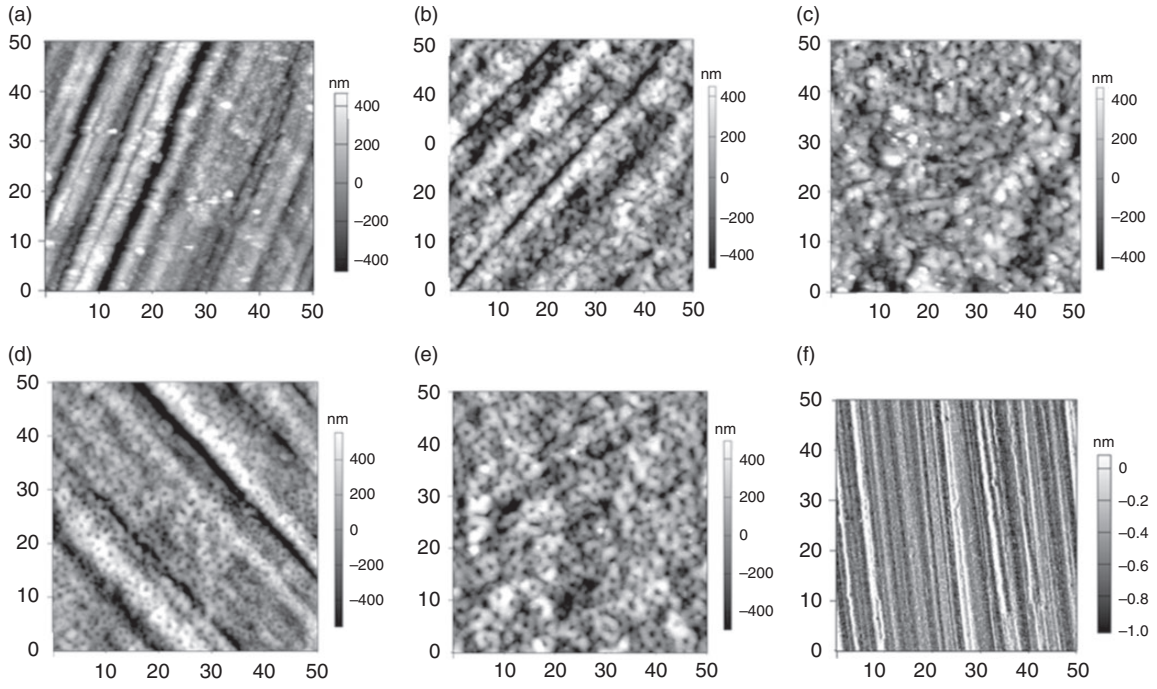

Figure 7. AFM micrographs (50 × 50 μm) of PEO-treated Mg surfaces. NAF (a), HMT (b), MAN (c), NAF-HMT (d), NAF-MAN (e) and c.p Mg (f).
PEO: plasma electrolytic oxidation; NAF: sodium fluoride; HMT: hexamethylenetetramine; MAN: mannitol.

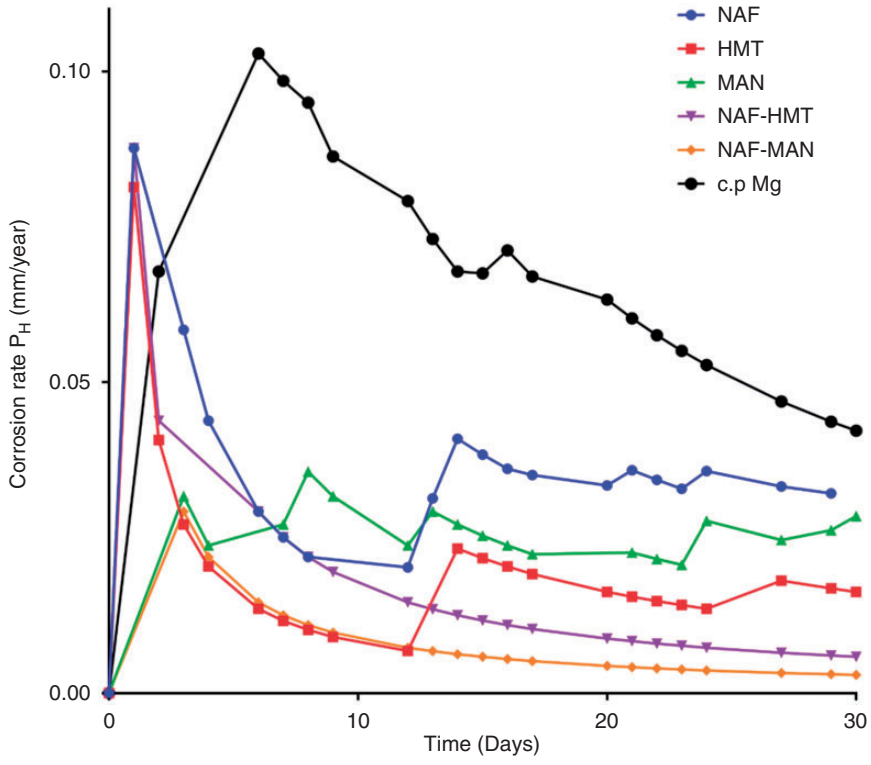

Figure 8. Corrosion of PEO-modified samples of Mg exposed to 0.9% m/v NaCl under hydrogen evolution assay.
PEO: plasma electrolytic oxidation.

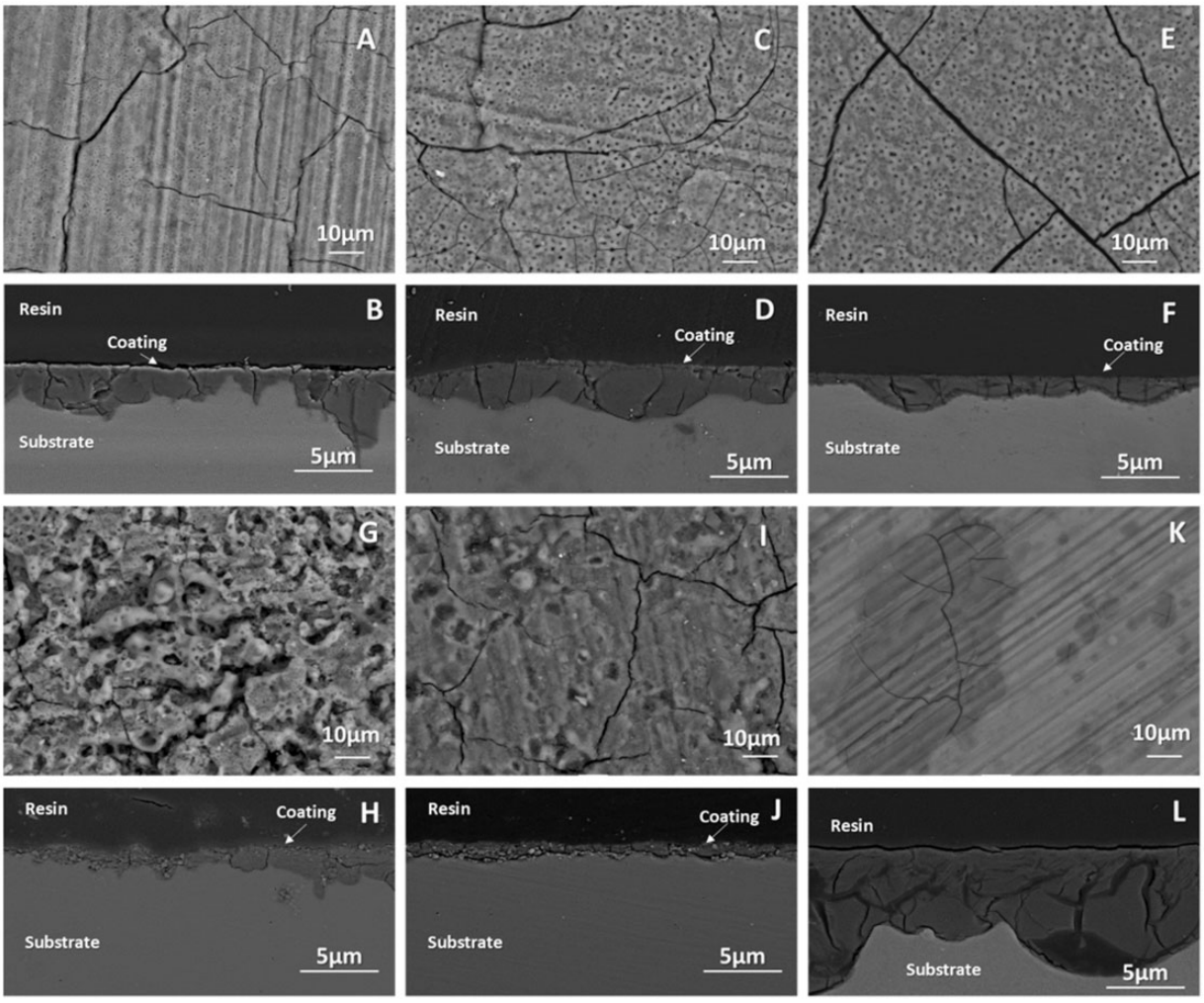

Figure 9. Surface and cross section of samples of PEO-modified Mg after 1 month of immersion in 0.9% (w/v) NaCl. NAF (a and b), HMT (c and d), MAN (e and f), NAF-HMT (g and h), NAF-MAN (i and j) and untreated sample (k and l).
PEO: plasma electrolytic oxidation; NAF: sodium fluoride; HMT: hexamethylenetetramine; MAN: mannitol.

area, 183 μm^2. The depth of the corrosion into the surface coating layer (Figure 9) and the respective area values calculated corroborated the corrosion rate as assessed hydrogen evolution (Figure 8). The NAF-MAN anodized sample exhibited the higher corrosion resistance, followed by the NAF-HMT and MAN samples and the lower corrosion resistances by NAF and HMT samples.

Biological assessments

In general, proliferation of sentinel cells (fibroblasts) on all surfaces was reduced compared to tissue culture plastic (Figure 10). Result of cytotoxicity test shows in Figure 10 that cells in the coatings with a single anodizing had less mitochondrial activity, which correlates with the rapidly increased initial corrosion rates of these surface coatings. However, cytotoxicity was not compromised for samples with two-step coatings. It should be noted that the variation was too large to confirm statistically significant differences between HTM and MAN and NAF-HMT surface coatings, yet the trend was present. Moreover, bare c.p Mg was highly cytotoxic.

The fractional difference in time was calculated between 24 h and 72 h culture. Cells grown on NAF and c.p Mg showed a reduction in mitochondrial activity after 72 h; HMT, MAN and NAF-HMT did not show changes in the cell population and NAF-MAN had a similar response to the control (cells grown on tissue culture plastic).

Osteoblast-material interaction strongly depended on the surface coating of the materials. For the anodized samples in general, a typical stretched morphology of the osteoblast was observed after the actin staining (Figure 11). In particular on single anodized surfaces osteoblasts had adhered and progressed to form a

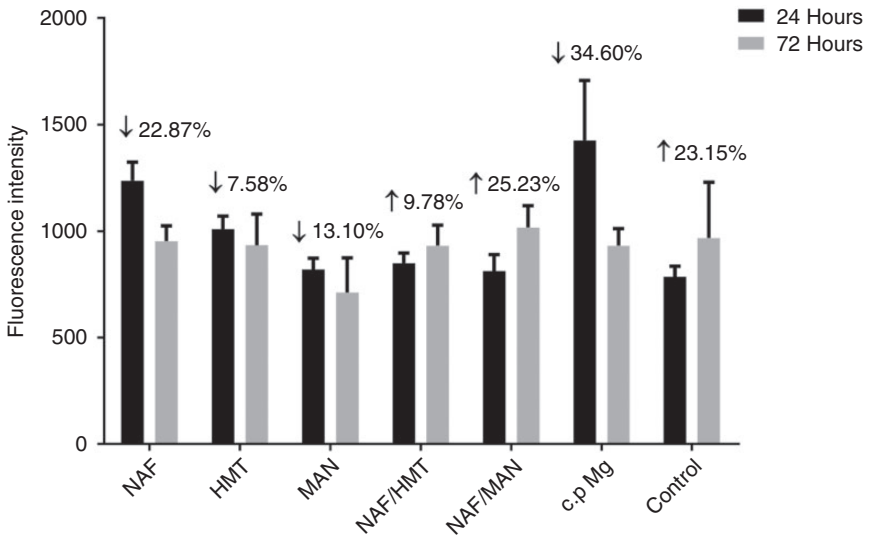

Figure 10. Proliferation of fibroblasts seeded on surface-coated Mg samples after 24 and 72 h.

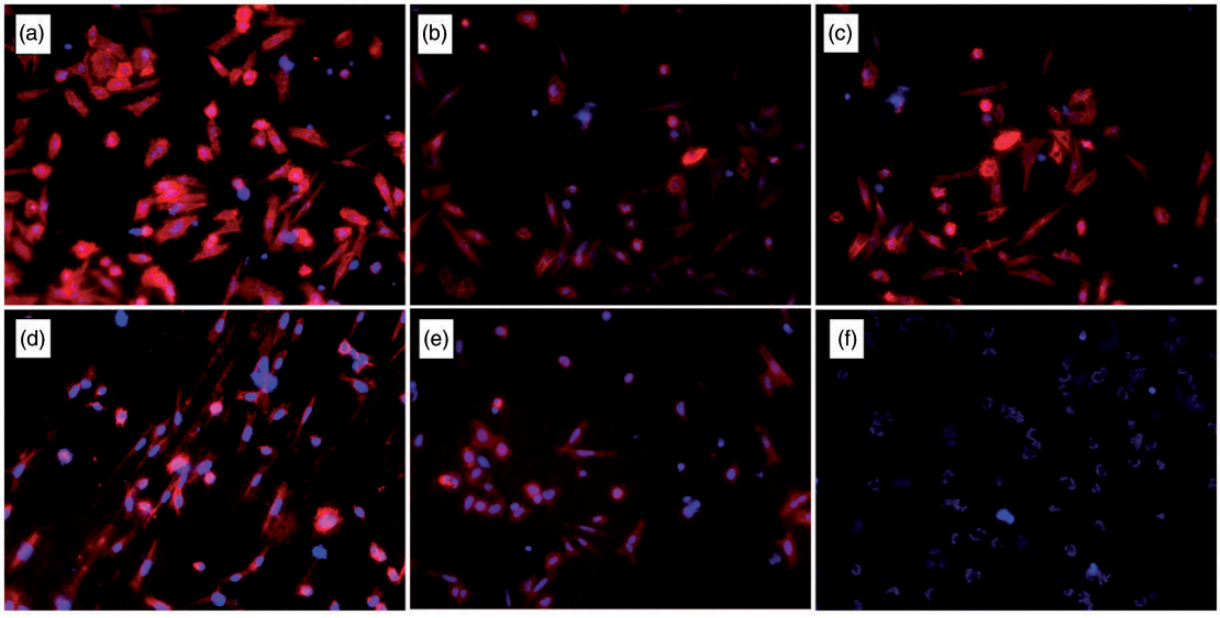

Figure 11. Cell-material interaction of osteoblasts with surface-coated Mg. Cytoskeleton of osteoblasts was stained with phalloidin (red) and nuclei with DAPI (blue). Adhered cells (red) were observed on samples NAF (a), HMT (b), MAN (c), NAF-HMT (d) and NAF-MAN (e), except for c.p Mg where only occasional fragmented nuclei were observed (f).
NAF: sodium fluoride; HMT: hexamethylenetetramine; MAN: mannitol.

monolayer, while on two-step anodized surface coatings, the apparent osteoblast density was lower. The highly cytotoxic c.p Mg did not allow cell survival and no more than fragmented nuclear remnants were discernable (Figure 11).

Irrespective of anodization all samples showed a high hemocompatiblity because no hemolysis occurred (Figure 12(a)) while no thrombin generation occurred (Figure 12(b and c) except for c.p Mg.

Discussion

Our results show that PEO treatment of c.p Mg yielded surface coatings of 3 to 4 μm thickness that all reduced the corrosion rate to biologically acceptable levels. This was virtually independent of additive, single or two-step PEO treatment and of anodization or cathodization. The surface topographies of the PEO-generated surfaces were comparable irrespective of treatment.

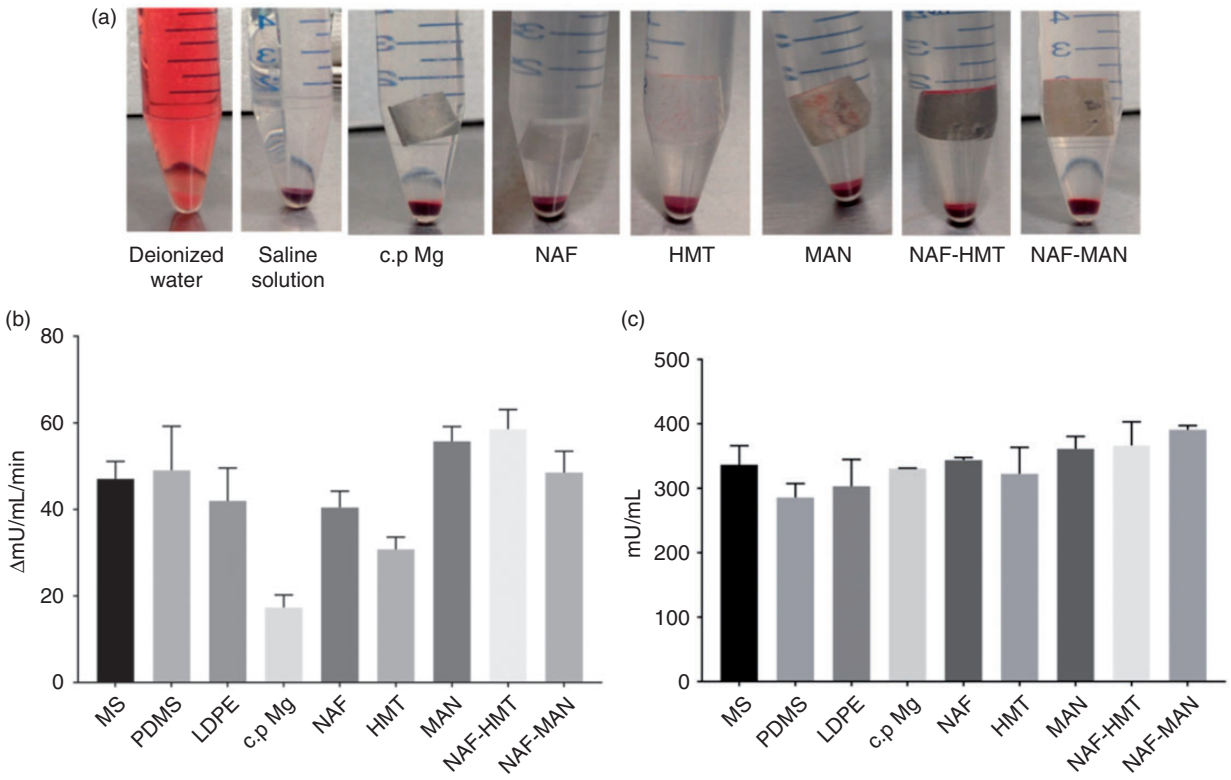

Figure 12. Hemocompatibility evaluation of PEO-modified Mg samples. (a) Hemolysis test, (b) speed of thrombin generation and (c) concentration of thrombin.

A major finding was that PEO increased the surface hydrophilicity and improved cell adhesion while reducing cytotoxicity. Studies carried out by Nguyen et al.[32] showed that surface roughness affect the corrosion resistance of Mg. Interestingly, they showed that smooth surfaces are more resistant than rough surfaces, which was explained by a higher penetrability of water into pores. Our data show that the topography itself is likely more influential on degradation, i.e. corrosion resistance, than the surface roughness. In addition to size and density of pores, another characteristic of the film that could affect its corrosion resistance could be the thickness of the barrier layer. However, our data showed no relationship with either of these parameters. Therefore, likely degradation is the result of combination of multiple, partly unknown, factors.

Our treatments, unexpectedly, did not reveal a correlation between wettability and corrosion resistance. According to the measurement of the contact angle and the calculation of the surface energy, uncoated Mg is hydrophobic; however, after the modification by PEO an improvement in the wettability of the surfaces was observed in all the specimens especially in the two-step coated surfaces which showed a 'superhydrophilic' behavior. These results are coherent according to what has been described by Zhang et al.,[33] who reported a contact angle of 46° for samples modified by PEO. In another study,[14] they showed that topography and roughness dictate the surface-free energy and wettability. To probe this, they studied changes in the contact angle in samples of abraded Mg at different grades. They concluded that at high roughness the increased available surface area allowed liquid interaction. This concept could be applicable to anodized samples of Mg, where the porous morphology increases the contact area. This is corroborated by NAF-generated surfaces which were compact and showed the highest contact angle and lower wettability in comparison with the other samples that mainly had porous surfaces.

Corrosion process may also be affected by the presence of impurities in the material causing differences in the standard electrode potential and producing microgalvanic corrosion.[34] The corrosion behavior of Mg also depends on the composition of the immersion solution. In the current study, NaCl was chosen as it is a highly corrosive medium; additionally, the concentration of chlorides is similar in simulated body fluid (SBF). Hydrogen evolution measurements were used to study the performance of the anodized Mg samples; for each mole of hydrogen produced, a mole of Mg was consumed.[19,35] For the case of biomedical applications,

it is expected that the response should be better because body fluids can be less aggressive that the solution employed here for testing (0.1 M NaCl).[36] After 1 month of immersion, the degradation rate for the c.p Mg was around 0.04 mm·year^{-1} while coated samples with a single anodic film decreased this value in around 50% and for the two-step anodized samples it was around 93%. Similar results were obtained by Xue et al.[37] who showed that c.p Mg anodized in silicate solution at different times decreased the degradation rate after its evaluation in NaCl solution and SBF. They show that anodization reduced the corrosion rate ten-fold in 2 h. They concluded that this is due to formation of oxide and silicon compounds that increase the thickness of the layer. Zhao et al.[38] anodized c.p Mg at galvanostatic mode in a solution of silicate with borate as additive and observed that the oxide film formed, which was composed mainly by Mg-borate compounds, has a critical anodizing time and above that point anodization reduces the corrosion resistance of the substrate instead of improving it. In our study, silicate compounds were only detected by XRD in the HMT sample, but EDS revealed the presence of Si in all anodic films. In addition, the formation of MgF_2 shown by XRD in the NAF-generated coatings, which could be an expected result and in agreement with other reports.[39,40] This fact, together with the EDS analysis of the NAF sample, indicates that the presence of fluoride ions in the electrolyte limits the introduction of silicate species into the film. A possible explanation of this result could be as follows. Although the change in Gibbs free energy for the formation of Mg_2SiO_4 is higher than for MgF_2,[41] considering the sizes of the silicate and fluoride ions, the mobility of the latter will be higher compared with the former and consequently the formation of MgF_2 will be favored over the Mg_2SiO_4 compound. In addition, as indicated by the EDS analysis of the two-step coatings, both HTM and MAN seems to preclude the introduction of fluoride ions into the anodic film. In all the coatings produced here, MgO appears to be the major constituent. On the other hand, as observed in the behavior of the corrosion rate vs time curves (Figure 7) and the cross sections of the samples after the immersion test (Figure 8), the corrosion products layer formed induces passivation of the surface. This passivation occurs within days for the anodized samples whilst it takes longer for bare Mg. Therefore, the reduction in the corrosion rate is a combined effect of the anodic film and the corrosion products layer formed underneath of it. Initially, the aggressive electrolyte species penetrate the anodic film through the pores, reaching the anodic film/substrate interface and reacting to form corrosion products, most possibly $Mg(OH)_2$. These products gradually 'grow' along this interface and possibly inside the pores, physically blocking the entrance of the electrolyte and consequently, thus, reducing the corrosion rate. This passivating process is less effective in bare Mg, as the corrosion products layer is not adherent and compact.

The use of a two-step anodization process, which starts with the formation of a film in NAF, introduces quite a lot of variations to the anodic oxide film performance, despite no differences being observed in the chemical composition of these films compared with the coatings formed by a single-step process. However, after the second anodizing process there was no evidence of fluoride in the oxide material and the content of Si was similar to the single anodized samples, while the coating thickness did not vary significantly. The surface morphology of the two-step coatings was similar to those of the HMT and MAN single anodized films, but differed from NAF. In addition, it appears that passing through porosity was larger for the single anodized samples. The two-step samples showed the higher wettability values (contact angles below 10°) and the lower corrosion rates of all the studied coatings. This all indicates that the initial anodic film containing F transforms during the second anodization into a different anodic layer with an increased corrosion resistance; however, using MAN in the second anodic process produces the coating with the lower corrosion rates.

The biological results in the present study showed that cells can grow in the modified surfaces while not on highly cytotoxic untreated Mg. The PEO-generated surface coatings were all hemocompatible. There are diverse investigations around the toxicity of Mg used for implants of bone and for cardiovascular stents and the use of PEO is one of the alternatives to improve its biological performance.[1] For instance, and according to Jo et al.,[42] the biocompatibility of Mg was improved by anodization technique as results of cell adhesion, DNA measurement and functional in vitro assays evidenced for osteoblasts when compared with results for bare c.p Mg. Additionally, Lin et al.[43] evaluated samples of a ZK60 Mg alloy anodized with an electrolytic solution similar to those studied in this work, in which a silicate base solution with fluoride additive was used; toxicity was measured by MTT assay obtaining positive results for the cells growing on the modified surfaces. Results from hemocompatibility assays obtained in the present work are in agreement with that of Li et al.,[44] who reported that even at higher concentrations of Mg^{2+} (10^{-3} M/L) hemolysis is not induced.

We have provided evidence that with tuning of PEO, the anodizing parameters allows to modulate the degradation rate of Mg. This is important for biomedical applications that require temporal implants, e.g. for

structural support.[45] These kind of materials are commonly used in orthopedics and cardiovascular fields.[46–51] One of the advantages to use these coatings is that the main components of the anodic film (MgO or Mg $(OH)_2$), once degraded in the body, do not cause adverse effects and are harmlessly excreted in the urine. In contrast, alloys that are designed to improve the mechanical properties and the corrosion resistance of Mg may also induce toxicity by the systemic accumulation of alloy elements such as aluminum.[52]

Conclusions

Plasma electrolytic oxidation deposits an oxide surface coating in a reproducible, controlled fashion and improves the corrosion resistance of Mg. Our study forwards HMT and MAN as promising additives to the electrolytic solution used to anodize c.p Mg. In addition, a two-step PEO improved both corrosion resistance and contact angle of surface coatings. Finally, surface coating by PEO improved hemocompatibility and reduced cytotoxicity of c.p Mg. These results indicate that two-step PEO of c.p Mg with HMT or MAN as electrolyte additives warrants further development to biomedical applications such as bone replacement and cardiovascular degradable stent.

Acknowledgements

The authors are pleased to acknowledge the financial assistance of COLCIENCIAS and Programa de Enlaza mundos 2015, which supported the PhD studies of MER.

Declaration of Conflicting Interests

The author(s) declared no potential conflicts of interest with respect to the research, authorship, and/or publication of this article.

Funding

The author(s) received no financial support for the research, authorship, and/or publication of this article.

ORCID iD

Monica Echeverry-Rendon http://orcid.org/0000-0002-7452-0987

References

1. Hornberger H, Virtanen S and Boccaccini AR. Biomedical coatings on magnesium alloys - a review. *Acta Biomater* 2012; 8: 2442–2455.
2. Sankara Narayanan TSN, Park IS and Lee MH. Strategies to improve the corrosion resistance of microarc oxidation (MAO) coated magnesium alloys for degradable implants: Prospects and challenges. *Prog Mater Sci* 2014; 60: 1–71.
3. Narayanan TSNS, Park IS and Lee MH. Progress in materials science strategies to improve the corrosion resistance of microarc oxidation (MAO) coated magnesium alloys for degradable implants: prospects and challenges. 2014; 60: 1–71.
4. Dong H. *Surface engineering of light alloys: aluminium, magnesium and titanium alloys*. Elsevier, 2010.
5. Yabuki A and Sakai M. Anodic films formed on magnesium in organic, silicate-containing electrolytes. *Corros Sci* 2009; 51: 793–798.
6. Salami B, Afshar A and Mazaheri A. The effect of sodium silicate concentration on microstructure and corrosion properties of MAO-coated magnesium alloy AZ31 in simulated body fluid. *J Magnes Alloy* 2014; 2: 72–77.
7. Hai-Lan W, Ying-Liang C, Ling-Ling L, et al. The anodization of ZK60 magnesium alloy in alkaline solution containing silicate and the corrosion properties of the anodized films. 2007; 253: 9387–9394.
8. Arrabal R, Matykina E, Viejo F, et al. Corrosion resistance of WE43 and AZ91D magnesium alloys with phosphate PEO coatings. 2008; 50: 1744–1752.
9. Liu Y, Yang F, Zhang Z, et al. Plasma electrolytic oxidation of AZ91D magnesium alloy in biosafety electrolyte for the surgical implant purpose. *Russ J Electrochem* 2013; 49: 987–993.
10. Stojadinović S, Vasilić R, Petković M, et al. Characterization of the plasma electrolytic oxidation of titanium in sodium metasilicate. *Appl Surf Sci* 2013; 265: 226–233.
11. Zhang RF, Zhang SF, Shen YL, et al. Applied surface science influence of sodium borate concentration on properties of anodic coatings obtained by micro arc oxidation on magnesium alloys. *Appl Surf Sci* 2012; 258: 6602–6610.
12. Yan LIU, Fu-Wei Y, Zhong-Ling WEI, et al. Anodizing of AZ91D magnesium alloy using environmental friendly alkaline borate-biphthalate electrolyte. *Trans Nonferrous Met Soc China* 2012; 22: 1778–1785.
13. Sreekanth D, Rameshbabu N and Venkateswarlu K. Effect of various additives on morphology and corrosion behavior of ceramic coatings developed on AZ31 magnesium alloy by plasma electrolytic oxidation. *Ceram Int* 2012; 38: 4607–4615.
14. Zhang X, Ma Q, Dai Y, et al. Effects of surface treatments and bonding types on the interfacial behavior of fiber metal laminate based on magnesium alloy. *Appl Surf Sci* 2018; 427: 897–906.
15. Jiang BL and Ge YF. Micro-arc oxidation (MAO) to improve the corrosion resistance of magnesium (Mg) alloys. In: Guang-Ling Song (ed) *Corrosion prevention of magnesium alloys*. New York: Woodhead Publishing, 2013, pp. 163–196.
16. Gao Y, Yerokhin A and Matthews A. Applied surface science effect of current mode on PEO treatment of

magnesium in Ca- and P-containing electrolyte and resulting coatings. *Appl Surf Sci* 2014; 316: 558–567.
17. Galvis OA, Quintero D, Castaño JG, et al. Formation of grooved and porous coatings on titanium by plasma electrolytic oxidation in H_2SO_4/H_3PO_4 electrolytes and effects of coating morphology on adhesive bonding. *Surf. Coatings Technol.* 2015; 269: 238–249.
18. Yao Z, Jiang Y, Jia F, et al. Growth characteristics of plasma electrolytic oxidation ceramic coatings on Ti–6Al–4V alloy. *Appl Surf Sci* 2008; 254: 4084–4091.
19. Jang Y, Tan Z, Jurey C, et al. Systematic understanding of corrosion behavior of plasma electrolytic oxidation treated AZ31 magnesium alloy using a mouse model of subcutaneous implant. *Mater Sci Eng C Mater Biol Appl* 2014; 45: 45–55.
20. Żenkiewicz M. Comparative study on the surface free energy of a solid calculated by different methods. *Polym Test* 2007; 26: 14–19.
21. Żenkiewicz M. Methods for the calculation of surface free energy of solids. *J Achiev Mater Manuf Eng* 2007; 24: 137–145.
22. Cappelletti G, Ardizzone S, Meroni D, et al. Wettability of bare and fluorinated silanes: a combined approach based on surface free energy evaluations and dipole moment calculations. *J Coll Interface Sci* 2013; 389: 284–291.
23. Matykina E, Garcia I, de Damborenea JJ, et al. Comparative determination of TiO_2 surface free energies for adhesive bonding application. *Int J Adhes* 2011; 31: 832–839.
24. Zhao Q, Liu Y and Abel EW. Effect of temperature on the surface free energy of amorphous carbon films. *J Coll Interface Sci* 2004; 280: 174–183.
25. Kwok DY. The usefulness of the Lifshitz–van der Waals/acid–base approach for surface tension components and interfacial tensions. *Coll Surf A Physicochem Eng Asp* 1999; 156: 191–200.
26. Schuster JM, Schvezov CE and Rosenberger MR. Analysis of the results of surface free energy measurement of Ti6Al4V by different methods. *Procedia Mater Sci* 2015; 8: 732–741.
27. Kirkland NT, Birbilis N and Staiger MP. Assessing the corrosion of biodegradable magnesium implants: a critical review of current methodologies and their limitations. *Acta Biomater* 2012; 8: 925–936.
28. Zakiyuddin A, Yun K and Lee K. Corrosion behavior of as-cast and hot rolled pure magnesium in simulated physiological media. *Met Mater Int* 2014; 20: 1163–1168.
29. Shi Z and Atrens A. An innovative specimen configuration for the study of Mg corrosion. *Corros Sci* 2011; 53: 226–246.
30. Song G, Atrens A and StJohn D. An hydrogen evolution method for the estimation of the corrosion rate of magnesium alloys. *Magnes Technol* 2001; 2001: 254–262.
31. Wang C, Jiang B, Liu M, et al. Corrosion characterization of micro-arc oxidization composite electrophoretic coating on AZ31B magnesium alloy. *J. Alloys Compd* 2015; 621: 53–61.
32. Nguyen TL, Blanquet A, Staiger MP, et al. On the role of surface roughness in the corrosion of pure magnesium in vitro. *J Biomed Mater Res Part B Appl Biomater* 2012; 100: 1310–1318.
33. Zhang Y, Feyerabend F, Tang S, et al. A study of degradation resistance and cytocompatibility of superhydrophobic coating on magnesium. *Mater Sci Eng C* 2017; 78: 405–412.
34. Fajardo S and Frankel GS. Effect of impurities on the enhanced catalytic activity for hydrogen evolution in high purity magnesium. *Electrochim Acta* 2015; 165: 255–267.
35. Frankel GS, Samaniego A and Birbilis N. Evolution of hydrogen at dissolving magnesium surfaces. *Corros Sci* 2013; 70: 104–111.
36. Hansen DC. Metal corrosion in the human body: the ultimate bio-corrosion scenario. *Electrochem Soc Interface* 2008; 17: 31.
37. Xue D, Yun Y, Schulz MJ, et al. Corrosion protection of biodegradable magnesium implants using anodization. *Mater Sci Eng C* 2011; 31: 215–223.
38. Zhao L, Cui C, Wang Q, et al. Growth characteristics and corrosion resistance of micro-arc oxidation coating on pure magnesium for biomedical applications. *Corros Sci* 2010; 52: 2228–2234.
39. Habazaki H, Kataoka F, Shahzad K, et al. Growth of barrier-type anodic films on magnesium in ethylene glycol electrolytes containing fluoride and water. *Electrochim Acta* 2015; 179: 402–410.
40. Jiang HB, Wu G, Lee S-B, et al. Achieving controllable degradation of a biomedical magnesium alloy by anodizing in molten ammonium bifluoride. *Surf Coatings Technol* 2017; 313: 282–287.
41. Richard A and Robie DRW. Thermodynamic properties of minerals and related substances at 298.15 K and 1 bar (10^5 pascals) pressure and at higher temperatures. US Government Printing Office: Volume (2131), 1995.
42. Jo J-H, Hong J-Y, Shin K-S, et al. Enhancing biocompatibility and corrosion resistance of Mg implants via surface treatments. *J Biomater Appl* 2012; 27: 469–476.
43. Lin X, Tan L, Zhang Q, et al. The in vitro degradation process and biocompatibility of a ZK60 magnesium alloy with a forsterite-containing micro-arc oxidation coating. *Acta Biomater* 2013; 9: 8631–8642.
44. Li R-C and Liu M. Effect of metal ions on human red blood cell membrane and its relationship with the metal ion properties. *J Beijing Med. Univ. (in Chinese)* 1995; 27: 239–240.
45. Witte F. The history of biodegradable magnesium implants: a review. *Acta Biomater* 2010; 6: 1680–1692.
46. Cabrejos-Azama J, Alkhraisat MH, Rueda C, et al. Magnesium substitution in brushite cements for enhanced bone tissue regeneration. *Mater Sci Eng C Mater Biol Appl* 2014; 43: 403–410.
47. Henderson SE, Verdelis K, Maiti S, et al. Magnesium alloys as a biomaterial for degradable craniofacial screws. *Acta Biomater* 2014; 10: 2323–2332.

48. Dorozhkin SV. Calcium orthophosphate coatings on magnesium and its biodegradable alloys. *Acta Biomater* 2014; 10: 2919–2934.
49. Galvin E, Morshed MM, Cummins C, et al. Surface modification of absorbable magnesium stents by reactive ion etching. *Plasma Chem Plasma Process* 2013; 33: 1137–1152.
50. Ma J, Zhao N, Betts L, et al. Bio-adaption between magnesium alloy stent and the blood vessel: a review. *J Mater Sci Technol* 2016; 32: 815–826.
51. Barlis P, Tanigawa J and Di Mario C. Coronary bioabsorbable magnesium stent: 15-month intravascular ultrasound and optical coherence tomography findings. *Eur. Heart J* 2007; 28: 2319
52. Seitz J-M, Eifler R, Bach F, et al. Magnesium degradation products: effects on tissue and human metabolism. *J Biomed Mater Res* 2014; 102: 3744–3753.